Journal of Colloid and Interface Science 354 (2011) 577–584

Contents lists available at ScienceDirect

Journal of Colloid and Interface Science

www.elsevier.com/locate/jcis

Ultrafast growth of dendritic gold nanostructures and their applications in methanol electro-oxidation and surface-enhanced Raman scattering

Xinyi Han, Dawei Wang, Jianshe Huang, Dong Liu, Tianyan You *

State Key Laboratory of Electroanalytical Chemistry, Changchun Institute of Applied Chemistry, Chinese Academy of Sciences, Changchun, Jilin 130022, People's Republic of China

ARTICLE INFO

Article history:
Received 15 September 2010
Accepted 17 November 2010
Available online 23 November 2010

Keywords:
Dendritic gold nanostructure
Methanol
Electro-oxidation
SERS

ABSTRACT

A simple and rapid solution-phase synthesis of dendritic gold nanostructures with hyperbranched architecture is demonstrated in this report. Further investigations revealed that the morphology of the synthesized sample depended on proper parameters such as reagent concentration, reaction temperature, reagent addition sequence and stir. Moreover, the dendritic gold nanostructures exhibited a good electrocatalytic activity toward methanol electro-oxidation. When compared with sea-urchinlike and flowerlike gold nanostructures which were prepared by varying the parameters of experiment, dendritic gold nanostructures showed the highest surface-enhanced Raman scattering (SERS) sensitivity using 4-aminothiophenol (4-ATP) as probe molecules. The dendritic gold nanostructures may find potential applications in catalysis, SERS and biosensor.

1. Introduction

Recently, the synthesis of noble metal nanostructures with uniform sizes and morphologies have become a central issue in modern material chemistry research not only because the physicochemical and optoelectronic properties of these nanostructures strongly depend on their size and shape [1,2] but also because they have potential applications ranging from catalysis to electronics, optics, sensor, and nanodevices [3–5]. In particular, gold nanostructures with controllable shapes have attracted great research interest as a result of their unique electrical and optical properties [6–9]. To date, most of the reports on controlling synthesis of gold nanostructures have focused on simple shapes, such as spheres [10], cubes [11,12], octahedral [12], tetrahedral [13], decahedra [14], rod [15], wire [16], belts [17], and plates [18].

Complex morphologies such as dendrites have potential applications in photoluminescence [19], catalysis [20–22], and SERS [23,24], but the synthesis of them still remain limited because of their highly symmetric face-centered cubic (fcc) crystal structure. Only in recent years, synthesis of dendritic gold nanostructures has received active research attention. Wang's group [19] and Dong's group [20] prepared dendritic gold nanostructures using an electrochemical method, respectively. Qi et al. [21] prepared dendritic gold nanostructures in DTAB/β-cyclodextrin aqueous solutions. Jiang et al. [23] obtained dendritic gold nanoparticles in one pot hydrothermal process via reduction of tetrachloroaurate by ammonium formate in the presence of poly (N-vinyl-2-pyrrolidone). Shi and coworkers [24] synthesized dendritic gold nanostructures at the aqueous/organic interface using 3,4-ethylenedioxythiophene as reductant. Selvan [25] synthesized dendritic gold nanostructures by vapor phase polymerization of pyrrole onto solution-cast films of block copolymer ionomers. Xie et al. [26] fabricated dendritic gold nanostructures in mixed cetyltrimethylammonium bromide and dodecyl sulfate sodium solutions. It has been reported that dendrimer-like gold nanoparticle assemblies could be obtained in $CF_3(CF_2)_7–SO_2NH–(CH_2)_3N^+(CH_3)_3I^-$ (HFOTAI) aqueous solution [27]. However, only a few literatures are available on facile synthesis of dendritic gold nanostructures with hyperbranched type and single crystalline [21,22]. Therefore, it would be highly desirable to develop a simple, rapid and low-cost method for the synthesis of single crystalline dendritic gold nanostructures with hyperbranched architecture in aqueous solutions.

Herein, we report a simple and rapid one-pot solution synthesis of single crystalline dendritic gold nanostructures with hyperbranched architecture at room temperature by reducing $HAuCl_4$ using ascorbic acid (AA) in aqueous solution of poly diallyl dimethyl ammonium chloride (PDDA). By changing the concentration of PDDA and $HAuCl_4$, sea-urchinlike and flowerlike nanostructures were obtained. The dendritic gold nanostructures exhibited high electrocatalytic activity towards the electro-oxidation of methanol which may have potential application in direct methanol fuel cell (DMFC). Furthermore, dendritic gold nanostructures show higher SERS activity than those of sea-urchinlike and flowerlike nanostructures.

* Corresponding author. Fax: +86 431 85262850.
E-mail address: youty@ciac.jl.cn (T. You).

0021-9797/$ - see front matter © 2010 Elsevier Inc. All rights reserved.
doi:10.1016/j.jcis.2010.11.045

2. Materials and methods

2.1. Materials

$HAuCl_4{\cdot}4H_2O$, and ascorbic acid (AA) were purchased from Shanghai Chemistry Co., Ltd. (China). Poly diallyl dimethyl ammonium chloride (PDDA, 50 wt.% in H_2O, M_w = 20 000) was obtained from Sigma–Aldrich. Methanol (CH_3OH) and potassium hydroxide (KOH) were purchased from Beijing Chemical Factory (Beijing, China). 4-Aminothiophenol (4-ATP) was obtained from Acros. All chemicals were used without further purification. The water used throughout the experiments was double distilled water.

2.2. Synthesis of dendritic gold nanostructures

For synthesis of dendritic gold nanostructures, 50 μL of 500 mM PDDA (on the basis of the molecular weight of the repeat unit) was added into 9.35 mL of water, followed by adding 0.5 mL of 10 mM $HAuCl_4{\cdot}4H_2O$ with stirring for 5 min. Then 0.1 mL of 100 mM freshly prepared AA was added dropwise. The reaction lasted for 2 min under stirring. The resultant hydrosols were purified by repeated centrifugation at 13,000 rpm for 10 min followed by redispersion of the residues in water to remove excess reagents. The temperature was controlled at 30 °C throughout the process.

2.3. Apparatus

A FEI XL30 ESEM FEG scanning electron microscope (SEM) was used to determine the morphology and composition of the products. Transmission electron microscopy (TEM) measurements and select area electron diffraction (SAED) pattern analysis were performed on a JEOL 2000 with an accelerating voltage of 200 kV. The sample for TEM characterization was prepared by placing a drop of prepared solution on a carbon-coated copper grid and dried at room temperature. UV–Vis absorption spectra were recorded with a Cary 50 UV–visible spectrophotometer (Varian, USA). X-ray diffraction (XRD) analysis was carried out on a D8 ADVANCE X-ray diffractometer using Cu (40 kV, 40 mA) radiation over a range of 20–80°. Cyclic voltammetric (CV) experiments were performed with a CHI 832 electrochemical analyzer (CH Instruments, Chenhua Co., Shanghai, China). A conventional three-electrode cell was used, including a Ag/AgCl (saturated KCl) electrode as reference electrode, a platinum wire as counter electrode, and a polycrystalline or modified polycrystalline gold as working electrode. The Raman instrument includes a Fourier transform Raman spectrometer (Thermo Nicolet 960) equipped with an InGaAs detector and a Nd/VO4 laser (1064 nm) as an excitation source. The resolution of the Raman instrument was ca. 4 cm^{-1} at the excitation wavelength used here, and the laser power used was about 300 mW, All FT-SERS were recorded by averaging 1024 scans.

2.4. Electrochemical experiments

Fifteen microliters of dendritic gold nanostructures (0.03 mg) were dropped on a commercial polycrystalline gold electrode and a clean glassy carbon electrode surface and allowed to dry at room temperature, respectively. For comparison, a commercial polycrystalline gold electrode was mechanically cleaned, electrochemically activated with sulfuric acid, and then used for electrochemical experiments. Methanol electrocatalytic oxidation measurements were performed in 0.1 M KOH solution. The measurements of the surface area of bare gold electrode and dendritic gold nanostructures modified electrode were performed in 0.5 M H_2SO_4 by cyclic voltammograms (CVs).

2.5. SERS measurements

First, the three differently shaped gold substrates (dendritic, sea-urchinlike and flowerlike nanostructures) solutions were centrifuged and redispersed in 1 mL of water. Then directly dropped the solution on the glass slides and allowed to dry in the air, respectively. At last, 5 μL of 10^{-5} M 4-ATP ethanol solution was dropped on the gold substrates and dried before Raman measurements.

3. Results and discussion

3.1. Structural characterization of dendritic gold nanostructures

Fig. 1 shows SEM images of typical dendritic nanostructures with different magnifications. As shown, the uniform and hyperbranched dendrites with stem in the length of about 0.5–1 μm were obtained. Fig. 1b reveals that the dendrites have several branches that grow radially away from a center. In each branch, there are plenty of secondary leaves grown on the stem, furthermore, the angle between the leave and the stem is about 60° and finally leading to the formation of dendrites.

The chemical composition of the dendritic nanostructures was determined by energy-dispersive X-ray spectroscopy (EDX) presented in Fig. 2a. As shown, the significant peaks associated with Au (Si and other peaks originated from ITO) can be observed, indicating high purity of the dendritic nanostructures. XRD analysis (Fig. 2b) was used to assess the overall quality, purity and crystal structure of the synthesized nanostructures. Four peaks associated with the [1 1 1], [2 0 0], [2 2 0] and [3 1 1] diffractions of the face-centered cubic (fcc) gold structure (JCPDS No. 04-0784) indicate

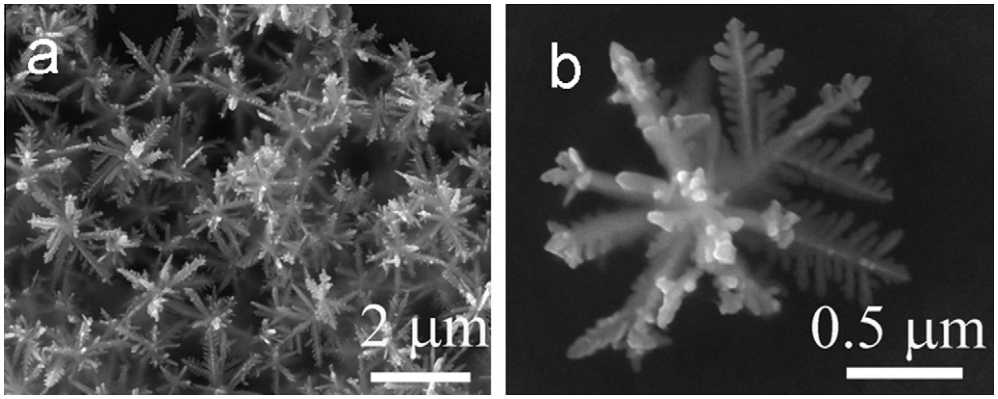

Fig. 1. SEM images of the dendritic gold nanostructures. (a) Low magnification. (b) High magnification.

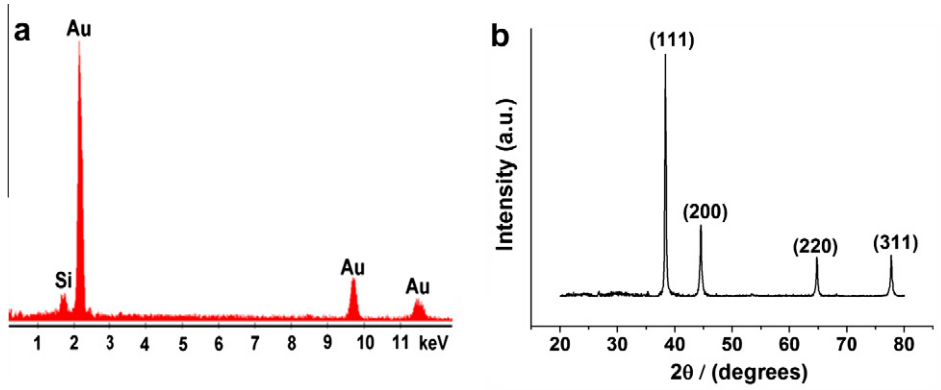

Fig. 2. EDX (a) and XRD (b) pattern of dendritic gold nanostructures.

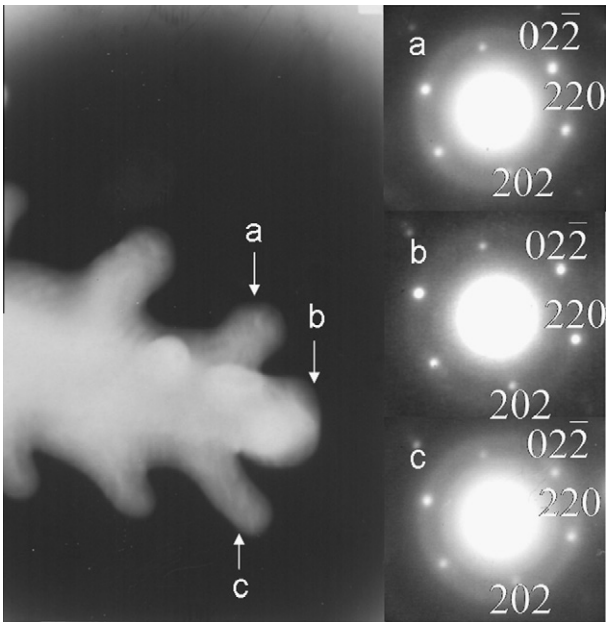

Fig. 3. TEM image of a dendrite and the selected area electron diffraction patterns of the leave (a), the stem (b), and the leave (c).

that the dendritic nanostructures are pure crystalline gold and have very high crystallinity.

Fig. 3 shows the TEM image of a dendrite and the corresponding elected area electron diffraction (SAED) patterns of the leave (a), the stem (b), and the leave (c). The obtained inerratic diffraction spots indicate that the leaves and stem of a dendrite are single crystalline structure. The diffraction spots of three parts can be approximatively indexed to the $[\bar{1}\,1\,1]$ zoneaxis of face-centered cubic crystal, suggested that the stem probably grows along $\langle 1\,1\,0\rangle$ direction and two leaves grow along $\langle 0\,1\,\bar{1}\rangle$ and $\langle 1\,0\,1\rangle$ directions, respectively.

3.2. Influence factors for the formation of dendritic gold nanostructures

3.2.1. Effect of PDDA concentration

It is well known that polyelectrolytes can be used as stabilizing agents for colloids owing to electrostatic stabilization [28]. As a class of water-soluble cationic polyelectrolyte, PDDA has been developed as a reducing and/or a stabilizing agent for the synthesis of Pt [29], Au [29,30], and Pd [31] nanoparticles. Generally, the reduction kinetics depends on reagent concentration [3] and the shape and size of the samples may be well controlled by varying the reagent concentration. Further experiments indicated that PDDA concentration played a key role in the formation of well-defined dendritic gold nanostructures. Fig. 4a–c shows SEM images of the obtained gold nanostructures at different PDDA concentrations (0–2.5 mM) without changing other parameters. When PDDA was absent (a), $HAuCl_4$ were reduced to Au atoms quickly, then random-shaped nanoparticles between 50 and 100 nm were obtained. When the concentration of PDDA was 0.5 mM, sea-urchinlike nanostructures (~500 nm) were prepared (b). While its concentration increased to 2.5 mM, the dendritic gold nanostructures were observed (c). When the concentration is higher than 5 mM (Supporting information Fig. S1), the dendritic gold nanostructures prepared were agglomerate. The experiments mentioned above proved that PDDA serves not only as a stabilizer but also a shape controller.

3.2.2. Effects of $HAuCl_4$ concentration and sequence of reagent added

Fig. 5a–c presents SEM images of the gold nanostructures synthesized at different $HAuCl_4$ concentrations (0.1–1.0 mM), by adding $HAuCl_4$ firstly and then adding AA into PDDA solution. Obviously, dendritic gold nanostructures were prepared at both of 0.1 mM (a) and 0.5 mM (b) $HAuCl_4$, though the dendrites prepared at (a) were smaller. In comparison, when the concentration of $HAuCl_4$ rose to 1.0 mM (c), the morphology became flowerlike.

It is interesting that the sequence of precursor and reductant also played a key role in the control of morphology. Fig. 5d shows the SEM image of samples when adding AA firstly and followed by adding $HAuCl_4$ into PDDA solution. In Fig. 5d, it can be seen that, the samples obtained changed into random-shaped nanoparticles in size of 100 nm. Similarly, Han' group [32] reported that cubic, multi-armed, and sea-urchinlike dendritic Pd nanoparticles could be selectively prepared when changing the adding sequence of reductant and polymer. As well known, PDDA and $AuCl_4^-$ ions could form stable ion pairs because of their electrostatic interaction, therefore, the reduction rate of $AuCl_4^-$ was decreased in the presence of PDDA [30]. It has been proved that anisotropic metal nanocrystals were favorable when the reaction rate was slow [33]. Under the slow reaction (a–c), the growth of gold nuclei could be kinetically controlled by the selective interactions between polymers and the different surface planes of gold nanocrystals, leading to the products deviated from the thermodynamically favored shapes. On the contrary (d), when adding AA firstly and followed by adding $HAuCl_4$ into PDDA solution, part of $HAuCl_4$ might be firstly reduced by AA before the formation of stable ion pairs between PDDA and $HAuCl_4$, resulting in a faster reduction rate and the isotropic gold nanoparticles were formed finally.

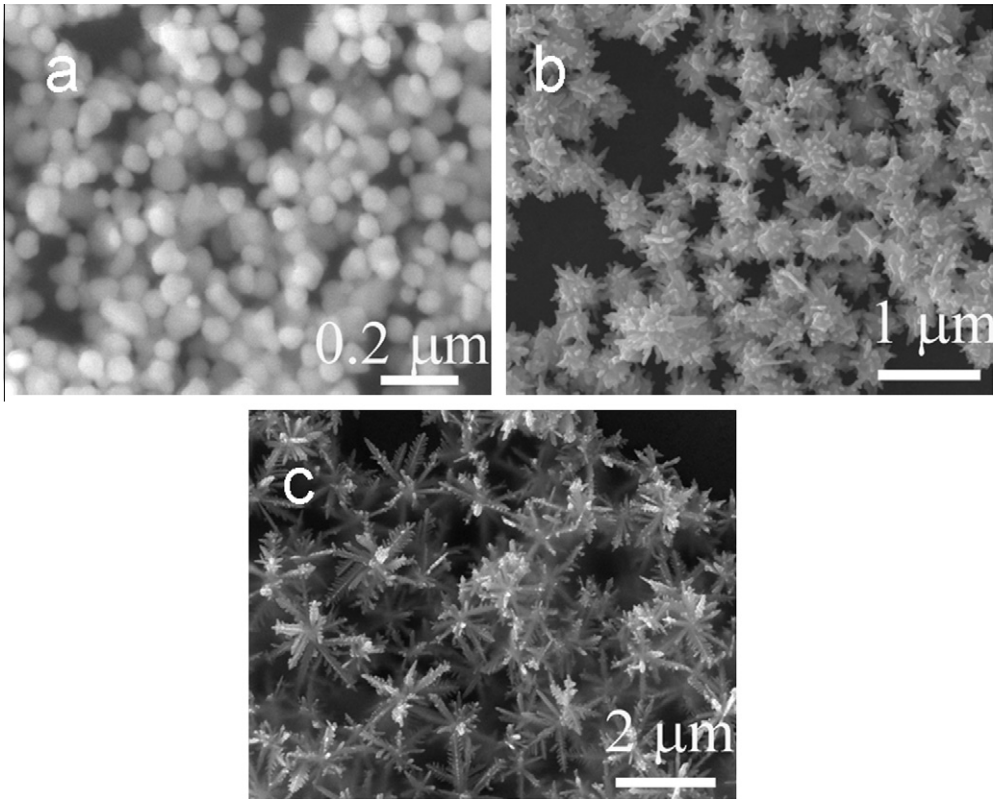

Fig. 4. SEM images of the nanostructures synthesized at different PDDA concentrations: (a) 0 mM, (b) 0.5 mM, and (c) 2.5 mM.

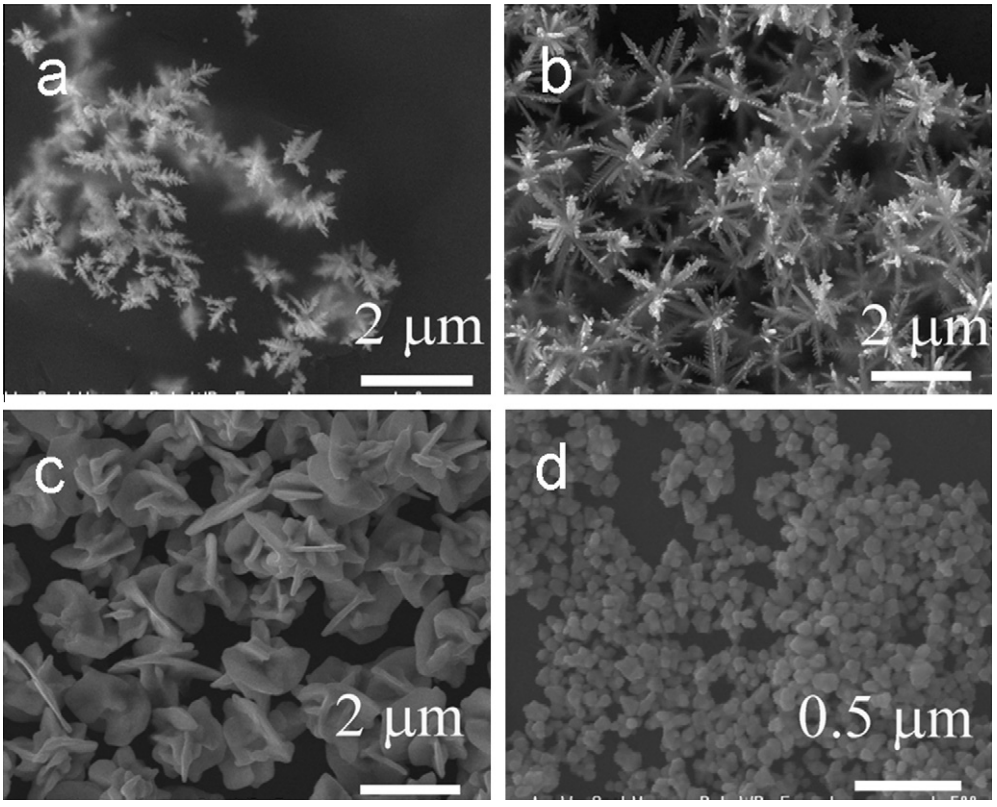

Fig. 5. (a–c) SEM images of samples when adding $HAuCl_4$ firstly and then adding AA into PDDA solution with different $HAuCl_4$ concentrations: (a) 0.1 mM, (b) 0.5 mM, and (c) 1.0 mM; (d). SEM image of sample when adding AA firstly and followed by adding $HAuCl_4$ into PDDA solution, the concentration of $HAuCl_4$ is 0.5 mM.

3.2.3. Effects of reaction temperature and stir

Besides reagent concentration, a proper reaction temperature of system is necessary for the preparation of dendritic gold nanostructures. Fig. 6a–c shows SEM images of the gold nanostructures synthesized at (a) 0 °C, (b) 30 °C, and (c) 60 °C under stirring condition. Fig. 6a shows that dendritic gold nanostructures with small size were prepared. As the temperature rises to 60 °C (Fig. 6c), quasi-spherical nanoparticles sized in hundreds nanometer were obtained. The reason may be ascribed to that: when the reaction temperature became higher, the growth of Au nuclei was controlled mainly by thermodynamics, so isotropic quasi-spherical gold nanoparticles were formed. Without stir, no dendrites but agglomerate nanoparticles were obtained (Fig. 6d). Wang's group [34] and Liz-Marzán's group [35] also reported that the maintenance of stir throughout the process was necessary for the preparation of dendritic nanostructures.

3.2.4. Effect of reaction time and possible mechanism

To investigate the nucleation and growth process of dendritic gold nanostructures, the reaction time of 20, 40, and 120 s were investigated. The representative SEM images of the products prepared at different reaction time intervals are shown in Fig. 7. These images illustrate the evolution of gold nanostructures from nanoparticles to dendrites. Congregated nanoparticles were formed at 20 s (a) and then served as nucleation sites for the further growth of anisotropic dendritic gold nanostructures. At the reaction time of 40 s (b), dendrites dominated the samples and no nanoparticles are observed, which indicates that initially produced nanoparticles had completely converted into dendrites. However, most of the stems are bald and only a few have secondary leaves growing out of them. At last, when the reaction time extended to 120 s (c), the perfect dendritic gold nanostructures with fully-grown leaves were synthesized. On the basis of these observations, a possible formation mechanism of dendritic gold nanostructures is described as follows: when AA was added to the solution of PDDA and $HAuCl_4$, gold atoms nucleated firstly. Then the followed growth of gold would preferentially occur on the preformed gold nuclei possibly due to the relatively high activation energy for the surface reaction, which resulted in dendrites with only a few stems having secondary leaves. Finally, more and more secondary leaves grew out of stems and formed complex dendritic gold nanostructures. The process is similar to the synthesis of dendritic gold nanostructure and gold and silver nanowire reported by Ding et al. [36] and Ramanath et al. [37], respectively. These results show that an oriented attachment based on the diffusion-limited growth process may be dominated the formation of dendritic gold nanostructures.

3.3. Electrocatalytic oxidation of methanol

It has been shown that gold nanostructures can exhibit good electrocatalytic activity for methanol oxidation and the catalytic property largely depends on their size and shape [22,38]. The synthesized dendritic gold nanostructures were deposited onto a commercial polycrystalline gold electrode to prepare gold dendrite electrode. Fig. 8 shows CVs of gold dendrite electrode (a) and bare gold electrode (b) in 0.5 M H_2SO_4. As shown, compared with bare gold electrode, the peak at 1.3 V is higher indicating that the surface may be dominated by [1 0 0] and [1 1 0] crystal plane [39]. After the modification, the surface area (0.102 cm^2) was nearly twice compared with bare gold electrode (0.056 cm^2), calculated by the charge consumed during the reduction of surface oxides using the value of 400 $\mu C/cm^2$ for a clean gold electrode [22].

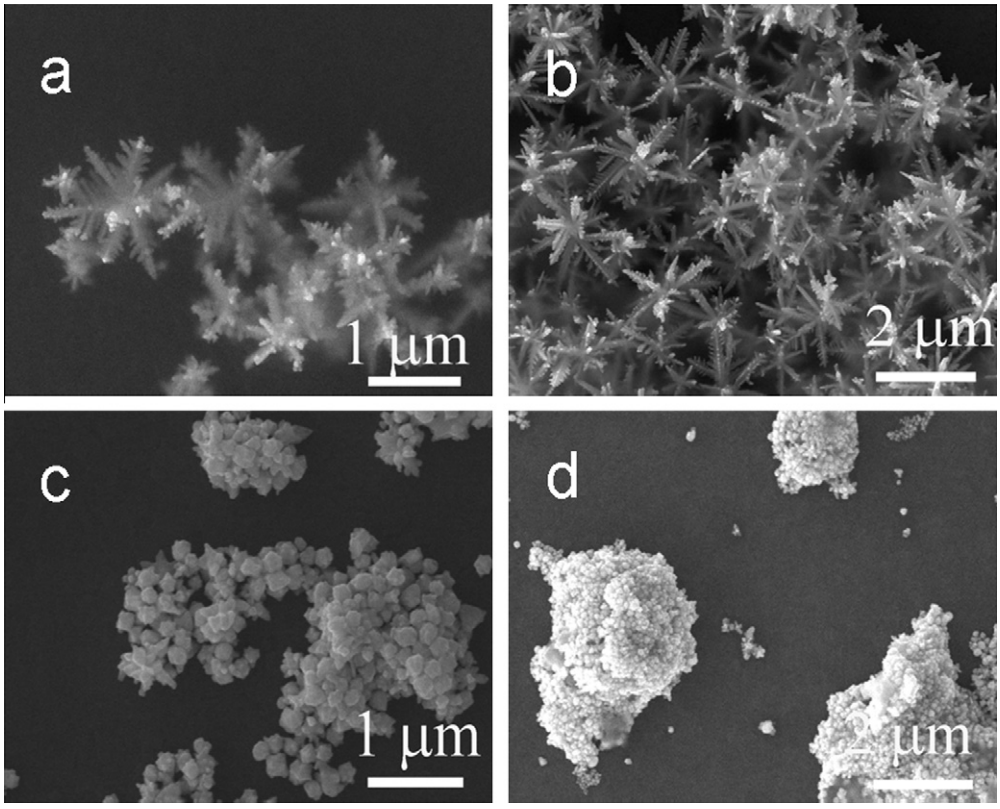

Fig. 6. (a–c) SEM images of the nanostructures synthesized at different reaction temperature: (a) 0 °C, (b) 30 °C, and (c) 60 °C, with stirring. (d) SEM image at 30 °C, without stirring.

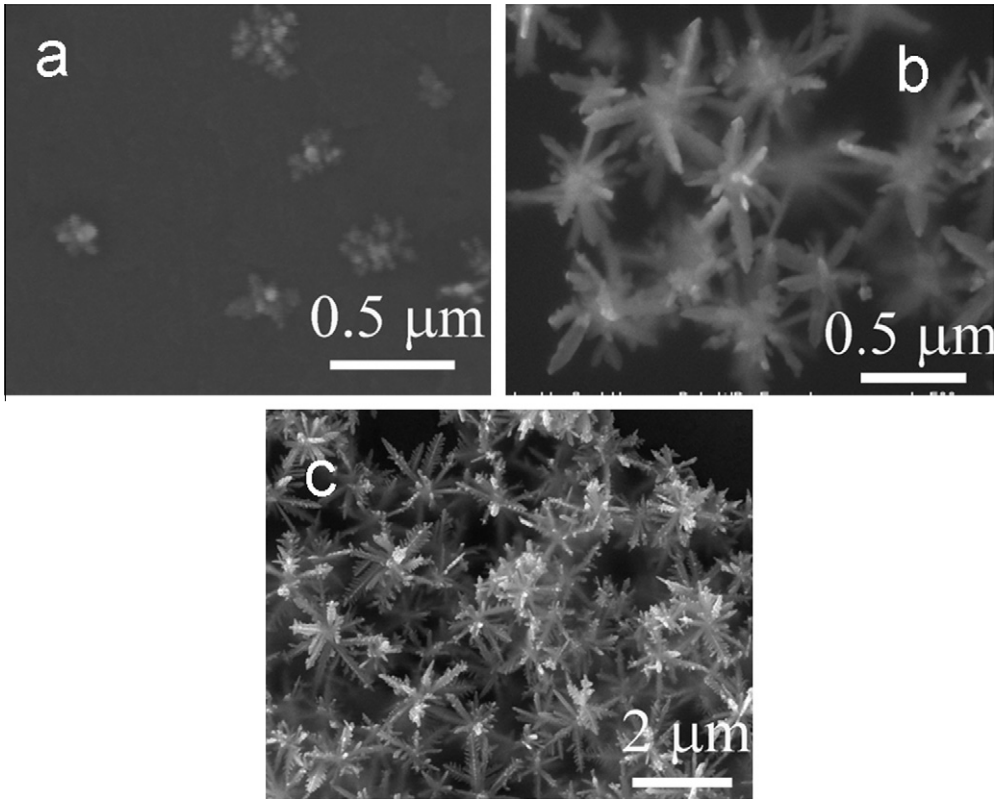

Fig. 7. SEM images of the nanostructures synthesized with different reaction time: (a) 20 s, (b) 40 s, and (c) 120 s.

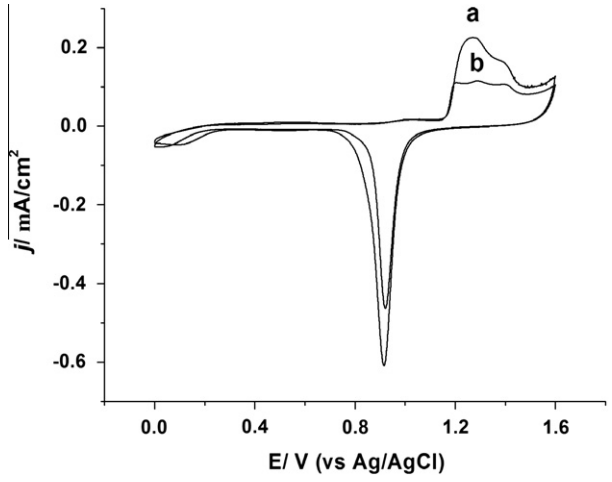

Fig. 8. Cyclic voltammograms of gold dendrite electrode (a) and bare gold electrode (b) in 0.5 M H_2SO_4, scan rate: 100 mV s^{-1}.

The electrocatalytic oxidation of methanol was investigated by CVs. Fig. 9 shows typical CVs of bare gold electrode (A) and gold dendrite electrode (B) in 0.1 M KOH solutions with (a) or without 1 M CH_3OH (b). The redox peaks at both electrodes in KOH can be ascribed to formation of gold oxides and subsequent the oxides reduction, respectively [21,22,38]. When 1 M methanol was added, the oxidation peak of methanol at gold dendrite electrode occurred at 0.337 V, which is 40 mV more negative than that at bare gold electrode (0.377 V). Moreover, the current density for the oxidation of methanol at gold dendrite electrode (95 μA/cm^2) is considerably larger than that at bare gold electrode (48 μA/cm^2). After the modification, the current density for the oxidation of methanol has enhanced nearly 99%, which is 30% larger than previous reports [21,22]. The lower oxidation potential and higher oxidation current density indicated that the gold dendrite electrode exhibited high electrocatalytic ability towards methanol oxidation. Generally, the higher electrocatalytic activity could be attributed to the specific morphology of dendrites contain numerous branches. It has been reported that high electrocatalytic activities towards methanol were observed at nested gold nanobelt electrode and gold dendrite electrode [21,38] due to more defects or hot spots and larger surface areas. Nevertheless, a further experiments need to be done to clarify the exact mechanism for the high electrocatalytic activity of the dendritic gold nanostructures.

In order to investigate whether the type of substrate electrode has an effect on the electro-oxidation of methanol, we modified the dendritic gold nanostructures on glassy carbon electrode. After the modification, the surface area was enhanced to 0.29 cm^2 (Supporting information Fig. S2). From the CVs of dendritic gold nanostructures modified glassy carbon electrode (Fig. 10) in KOH with (curve a) and without 1 M methanol (curve b), we can see that after methanol was added, a narrow methanol oxidation peak appeared at about 0.33 V. There is no distinct difference between the results of methanol electro-oxidation on dendritic gold nanostructures modified polycrystalline gold electrode (Fig. 9B) and modified glassy carbon electrode.

3.4. UV–Vis absorption spectra of the three differently shaped gold and their SERS of 4-ATP

Fig. 11 shows the UV–Vis absorption spectra of dendritic, flowerlike, and sea-urchinlike gold nanostructures. As shown, dendritic gold nanostructures display a gradual increase in absorption intensity from about 500 nm to the near-IR region, which could be ascribed to the longitudinal plasmon band. The result suggests an

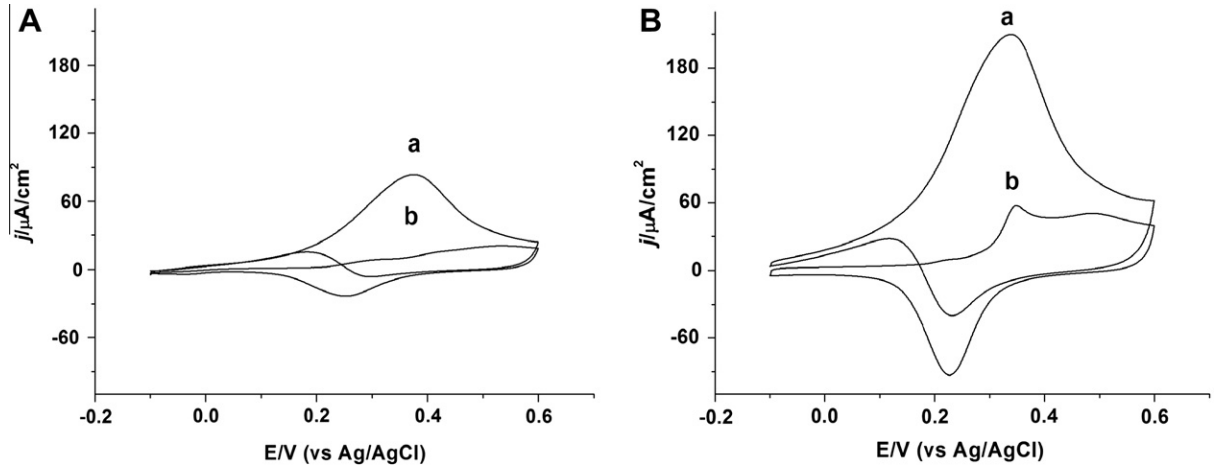

Fig. 9. Cyclic voltammograms of bare gold electrode (A) and gold dendrite electrode (B) in 0.1 M KOH solutions with (a) and without 1 M CH_3OH (b), scan rate: 10 mV s^{-1}.

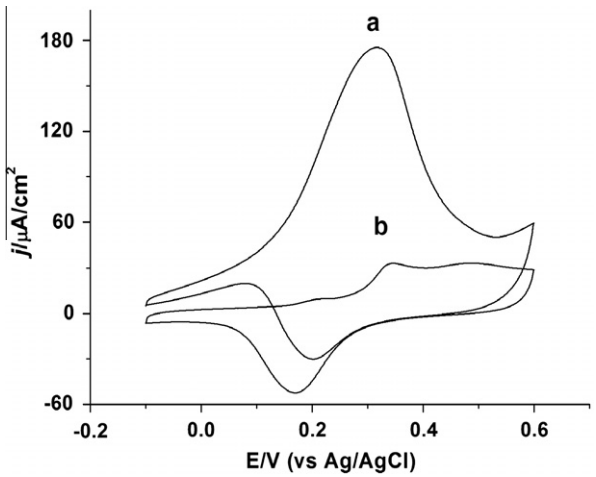

Fig. 10. Cyclic voltammograms of dendritic gold nanostructures modified glassy carbon electrode in 0.1 M KOH solutions with (a) and without 1 M CH_3OH (b), scan rate: 10 mV s^{-1}.

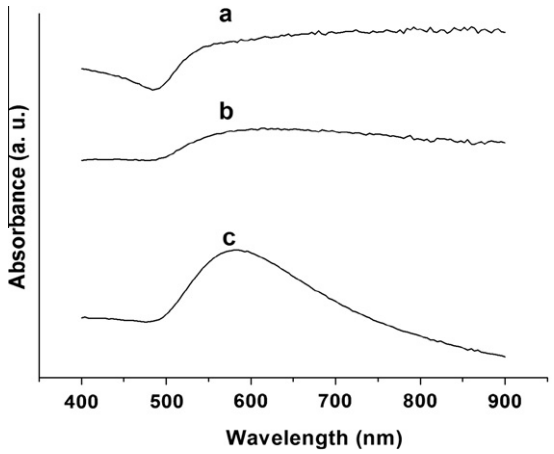

Fig. 11. UV–Vis absorption spectra of the three differently shaped gold nanostructures: (a) dendritic nanostructures, (b) flowerlike nanostructures, and (c) sea-urchinlike nanostructures.

unusual overlapping between the transverse band and the longitudinal band had happened. It is universally acknowledged that the surface plasmon resonance (SPR) absorption of gold nanostructures is dependent on the size, shape, and aspect ratio [40–42]. So the unusual overlapping between the transverse band and the longitudinal band might be due to the variety of sizes, aspect ratios and the various coupling between stems and branches of dendrites. The similar UV–Vis absorption spectrum has been reported by Qi's group [21]. Flowerlike gold nanostructures have a broad band at about 620 nm. The broad band and red-shift of SPR band compared with spherical gold nanoparticles indicate the prepared gold nanostructures had an anisotropic morphology or were larger in size than typical gold nanoparticles [43]. Sea-urchinlike gold nanostructures have a relatively narrow band at about 590 nm, which is the surface plasmon resonance band of gold crystals, indicating that gold crystals had formed. Because the SPR band of spherical nanoparticles falls between about 520 and 530 nm [44], the red-shifted SPR absorption indicates that the sample has a different morphology from spherical nanostructures [43,45]. The similar UV–Vis absorption spectra haven been reported by Han's group [45] and Lee's group [46].

Dendritic gold nanostructures could further serve as effective substrates for SERS detection because of their sharp edges or tips and their high surface areas. We used 4-ATP as a model molecule to investigate the SERS sensitivity of the flowerlike (a), sea-urchinlike (b) and dendritic (c) gold nanostructures. As shown in Fig. 12, the flowerlike gold nanostructure exhibits the lowest SERS activity (a), sea-urchinlike gold nanostructures exhibit higher SERS activity

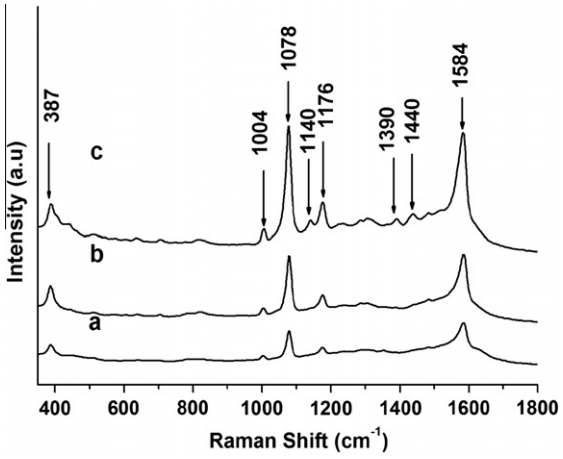

Fig. 12. FT-SERS spectra of 4-ATP (10^{-5} M) on different shape gold nanostructures: (a) flowerlike nanostructures, (b) sea-urchinlike nanostructures, and (c) dendritic nanostructures.

(b) and dendritic gold nanostructures exhibit the highest SERS activity (c).

It is clear that three SERS spectra are all dominant with a_1 vibration modes at 1078 and 1584 cm^{-1} [47]. The band at 387 cm^{-1} is assigned to one of the vibrational modes of the C–S bond, most likely the bending mode of the C–S bond [47]. The predominance of a_1 modes in these SERS spectra may imply that the enhancement via an electromagnetic mechanism is significant. Moreover, the enhancement of b_2 modes located at 1176 and 1004 cm^{-1} is also apparent, which was related to the charge transfer (CT) of the metal to the adsorbed molecules, indicating 4-ATP contact with the gold nanostructures surfaces by forming a strong Au–S bond [47]. Furthermore, the enhancement of b_2 modes located at 1440, 1390, and 1140 cm^{-1} [47] is also apparent on curve c, suggesting that a greater extent of charge transfer from the dendritic gold nanostructures to 4-ATP [48]. The higher SERS activity of dendritic gold nanostructures probably caused by their unique morphology and electromagnetic enhanced at sharp edges or tips.

4. Conclusion

In summary, a rapid and simple method for preparation of single crystalline dendritic gold nanostructures with hyperbranched architecture is presented by the reduction of $HAuCl_4$ with AA in PDDA aqueous solution at room temperature. The studies of the influence factors for the formation of dendritic gold nanostructures showed that the concentrations of $HAuCl_4$ and PDDA as well as the reaction temperature, the sequence of precursor and reductant added and stir played keys role in the process. Moreover, sea-urchinlike and flowerlike nanostructures could be obtained by changing the parameters of experiment. The possible formation mechanism of dendritic gold nanostructures was also discussed. The dendritic gold nanostructures exhibited both a good electrocatalytic activity toward the oxidation of methanol and higher SERS activity, indicating potential applications in catalysis, biosensing and SERS.

Acknowledgments

We gratefully acknowledge financial support from the National Natural Science Foundation of China (No. 20875085) and the Chinese Academy of Science (KJCX2-YW-H11).

Appendix A. Supplementary material

Supplementary data associated with this article can be found, in the online version, at doi:10.1016/j.jcis.2010.11.045.

References

[1] C. Burda, X.B. Chen, R. Narayanan, M.A. El-Sayed, Chem. Rev. 105 (2005) 1025.
[2] Y.N. Xia, N.J. Halas, Mater. Res. Soc. Bull. 30 (2005) 338.
[3] M.C. Daniel, D. Astruc, Chem. Rev. 104 (2004) 293.
[4] A.R. Tao, S. Habas, P.D. Yang, Small 4 (2008) 310.
[5] T.K. Sau, A.L. Rogach, F. Jäckel, T.A. Klar, F. Feldmann, Adv. Mater. 22 (2010) 1805.
[6] D.A. Stuart, A.J. Haes, C.R. Yonzon, E.M. Hicks, Nanotechnology 152 (2005) 13.
[7] S.J. Hurst, A.K.R. Lytton-Jean, C.A. Mirkin, Anal. Chem. 78 (2006) 8313.
[8] H. Tsunlyama, H. Sakurai, Y. Negishi, T. Tsukuda, J. Am. Chem. Soc. 127 (2005) 9374.
[9] S. Panigrahi, S. Basu, S. Praharaj, S. Pande, S. Jana, J. Phys. Chem. C 111 (2007) 4596.
[10] X. Wang, Q. Peng, Y. Li, Nature 437 (2005) 121.
[11] T.K. Sau, J. Murplhy, J. Am. Chem. Soc. 126 (2004) 8648.
[12] J. Zhang, Y. Gao, R.A. Puebla, J.M. Buriak, H. Fenniri, Adv. Mater. 18 (2006) 3233.
[13] F. Kim, S. Connor, Y. Kuykendall, P.D. Yang, Angew. Chem., Int. Ed. 43 (2004) 3673.
[14] J.H. Sun, M.Y. Guan, C.L. Gao, J.M. Zhu, Cryst. Growth Des. 8 (2008) 906.
[15] R. Becker, B. Liedberg, P.O. Käll, J. Colloid Interface Sci. 343 (2010) 25.
[16] E. Tosatti, S. Prestipino, Science 289 (2000) 561.
[17] J.L. Zhang, J.M. Du, Z.F. Zhang, Angew. Chem., Int. Ed. 45 (2006) 1116.
[18] J.U. Kim, S.H. Cha, K. Shin, J.C. Lee, Adv. Mater. 416 (2004) 59.
[19] Y. Hu, N. Pan, K. Zhang, Z. Wang, H. Hu, X. Wang, Phys. Status Solidi A 204 (2007) 3398.
[20] X.L. Xu, J.B. Jia, X.R. Yang, S.J. Dong, Langmuir 26 (2010) 7627.
[21] T. Huang, F. Meng, L.M. Qi, Langmuir 26 (2010) 7582.
[22] Q. Yao, S. Yin, N.J. Sun, N.N. Zhao, M.X. Li, L.M. Qi, Chem. Mater. 20 (2008) 3965.
[23] X.L. Tang, P. Jiang, G.L. Ge, M. Tsuji, S.S. Xie, Y.J. Guo, Langmuir 24 (2008) 1763.
[24] G.W. Lu, C. Li, G.Q. Shi, Chem. Mater. 19 (2007) 3433.
[25] S. Selvan, Chem. Commun. (1998) 351.
[26] X.W. Zheng, L.Y. Zhu, X.J. Wang, Ai.H. Yan, Y. Xie, J. Crystal Growth 260 (2004) 255.
[27] S.F. Pang, T.S. Kondo, T.S. Kawai, Chem. Mater. 17 (2005) 3636.
[28] T.L. Pugh, W. Heller, J. Polym. Sci. 47 (1960) 219.
[29] H.J. Chen, Y.L. Wang, S.J. Dong, Inorg. Chem. 46 (2007) 10587.
[30] C.C. Li, L. Kevin, M.H. Chen, S.O. Cho, ACS Nano 2 (2008) 1760.
[31] F.R. Fan, A. Attia, J.B. Chen, Z.Q. Tian, Cryst. Growth Des. 9 (2009) 2335.
[32] W.L. Lee, M.J. Kim, S.W. Han, Chem. Commun. 46 (2010) 1535.
[33] C.C. Li, W.P. Cai, B.Q. Cao, C.X. Kan, L.D. Zhang, Adv. Funct. Mater. 16 (2006) 83.
[34] G.H. Jiang, L. Wang, T. Chen, H.J. Yu, J.J. Wang, J. Mater. Sci. 40 (2005) 1681.
[35] P.S. Kumar1, I.P. Santos, L.M. Liz-Marźan, Nanotechnology 19 (2008) 015606.
[36] J.X. Fang, X.N. Ma, H.H. Cai, X.P. Song, B.J. Ding, Nanotechnology 17 (2006) 5841.
[37] T. Maddanimath, A. Kumar, K. Vijayamohanan, G. Ramanath, Chem. Commun. (2005) 1435.
[38] N. Zhao, Y. Wei, N. Sun, L. Zhou, Y. Qin, M. Li, L. Qi, Langmuir 24 (2008) 991.
[39] A. Hamelin, J. Electroanal. Chem. 407 (1996) 11.
[40] P.K. Jain, X. Huang, I.H. El-Sayed, M.A. El-Sayed, Acc. Chem. Res. 41 (2008) 1578.
[41] L. Gou, C. Murphy, J. Chem. Mater. 17 (2005) 3668.
[42] X. Xu, M. Cortie, Adv. Funct. Mater. 16 (2006) 2170.
[43] S.H. Cha, K.H. Kim, W.K. Lee, J.C. Lee, J. Solid State Chem. 182 (2009) 1575.
[44] S. Takami, T. Toshiharu, H. Satoshi, M. Mikio, J. Phys. Chem. B 107 (2003) 2719.
[45] G.H. Jeong, Y.W. Lee, M. Kim, S.W. Han, J. Colloid Interface Sci. 329 (2009) 97.
[46] J.P. Xie, Q.B. Zhang, J.Y. Lee, D.I.C. Wang, ACS Nano 2 (2008) 247.
[47] X.G. Hu, W.L. Cheng, T. Wang, E.K. Wang, S.J. Dong, J. Phys. Chem. B 109 (2005) 19385.
[48] J. Zheng, Y. Zhou, X. Li, Y. Ji, T. Lu, R. Gu, Langmuir 19 (2003) 632.